Çukurova Üniversitesi
Mühendislik Fakültesi Dergisi
Çukurova University
Journal of the Faculty of Engineering
ISSN: 2757-9255 CİLT/VOLUME: 41 SAYI/ISSUE: 1 MART/MARCH 2026

Spectral Analysis of Electric Vehicle Dynamics for Battery Eccentricity Using a Full-Car Model under Random Road Excitation

Hikmet BAL [1,a]

[1]*OSTIM Technical University, Faculty of Engineering, Department of Aerospace Engineering, Ankara, Türkiye*

[a]***ORCID**: 0000-0001-9062-6469*

Article Info
Received : 27.02.2026
Accepted : 23.03.2026
DOI: 10.21605/cukurovaumfd.1898814

Corresponding Author
Hikmet BAL
hikmet.bal@ostimteknik.edu.tr

Keywords
Vehicle dynamics
Electrical vehicle
Random vibrations
Spectral analysis
Battery eccentricity

***How to cite:** BAL, H., (2026). Spectral Analysis of Electric Vehicle Dynamics for Battery Eccentricity Using a Full-Car Model under Random Road Excitation. Cukurova University, Journal of the Faculty of Engineering, 41(1), 227-240.*

ABSTRACT

Electrical-vehicle (EV) dynamics are significantly influenced by battery mass and the location. Therefore, the combined investigation of a 7-DoF model, random road excitation, and eccentric battery effects is necessary for more accurate characterization of vehicle dynamics. In this study, a 7-DoF EV full-vehicle model considering battery eccentricity is derived to examine the coupled heave–roll–pitch vibrations under random road excitation. A spectral method is employed for the solution. EV response spectra are obtained using the power-spectral-density (PSD) of road roughness and the EV frequency-response-functions (FRFs). RMS values of response are investigated for different battery eccentricities and vehicle speeds [1-160km/h]. The results show that the normalized RMS varies up to ~30% total with EV speed and battery eccentricity. The highest RMS occur at vehicle speeds where the natural frequency is excited, while the lowest vibration RMS is obtained at low battery eccentricity on the x-axis. The developed EV model and solution method have been presented as a successful tool for investigating random vibrations and vehicle dynamics.

Elektrikli Araç Dinamiğinin Rastgele Yol Uyarısı Altında Tam Araç Modeli Kullanılarak Batarya Eksantrikliği için Spektral Analizi

Makale Bilgileri
Geliş : 27.02.2026
Kabul : 23.03.2026
DOI: 10.21605/cukurovaumfd.1898814

Sorumlu Yazar
Hikmet BAL
hikmet.bal@ostimteknik.edu.tr

Anahtar Kelimeler
Taşıt dinamiği
Elektrikli araç
Düzensiz titreşimler
Spectral analiz
Batarya eksantrikliği

***Atıf şekli:** BAL, H., (2026). Elektrikli Araç Dinamiğinin Rastgele Yol Uyarısı Altında Tam Araç Modeli Kullanılarak Batarya Eksantrikliği için Spektral Analizi. Çukurova Üniversitesi, Mühendislik Fakültesi Dergisi, 41(1), 227-240.*

ÖZ

Elektrikli araç (EV) dinamiği, batarya kütlesi, ağırlık merkezinin konumundan önemli ölçüde etkilenmektedir. Dolayısıyla, 7-DoF modellemesi, rastgele yol uyarımı ve eksantrik batarya yerleşimi etkilerinin birlikte incelenmesi, araç dinamiğinin daha net belirlenebilmesi için gerekliliktir. Bu çalışmada, farklı araç hızları ve rastgele yol uyarımı altında birleşik yükselme-eğilme-yuvarlanma titreşim tepkilerini incelemek için 7-DoF tam araç modeli, batarya eksantrikliği de dikkate alınarak türetilmiştir. Çözüm için spectral metot kullanılmıştır. EV tepki spektrumları, yol pürüzlülüğünün güç spectral yoğunluğu (PSD) ve EV frekans-cevabı-fonksiyonundan (FRF) elde edilmiştir. Farklı batarya eksantriklikleri ve araç hızları [1-160km/s] için araç titreşiminin RMS'i hesaplanarak, titreşim davranışı üzerindeki etkileri araştırılmıştır. Sonuçlar, titreşim normalize RMS'sinin araç hızı ve batarya eksantrikliği ile toplamda ~%30'a kadar değişimini göstermektedir. En yüksek RMS genlikleri doğal frekansın uyarıldığı araç hızlarında iken, en düşük titreşim RMS'i, batarya eksantrikliğinin az olduğu, x-ekseni üzerindeki, konularda elde edilmiştir. Geliştirilen EV modeli ve çözüm metodu düzensiz titreşimlerin ve araç dinamiğinin incelenmesinde başarılı bir araç olarak sunulmuştur.

1. INTRODUCTION

Vehicle ride quality, safety, and passenger comfort are fundamentally governed by vehicle dynamics, particularly the interaction between suspension systems and road surface irregularities. In electric vehicles, battery center-of-gravity location significantly influences dynamic behavior. Consequently, modern vehicle design requires comprehensive understanding of vibrational responses to random road excitation, especially as the automotive industry transitions toward electric vehicles with heavy battery packs and altered mass distributions. Accurate prediction of vehicle dynamics under stochastic road inputs demands sophisticated mathematical models and appropriate spectral analysis techniques for handling non-stationary random processes.

The literature reveals extensive application of vehicle dynamic modeling approaches, random vibration analysis methodologies, and spectral techniques. The quarter-car model, representing the fundamental building block of vehicle suspension analysis, captures essential vertical motion characteristics with minimal computational complexity. While widely used in vehicle dynamics studies, this formulation cannot capture pitch, roll, or coupling effects between multiple wheels, restricting its applicability to preliminary vertical dynamics investigations.

Karaçay et al. [1] employed a 2-DOF quarter-car model to investigate ride characteristics of vehicles traversing rough surfaces at varying speeds. Recognizing that vehicle dynamics under changing speeds presents a non-stationary random vibration problem—as statistical characteristics of temporal excitation vary with velocity—Karaçay et al. [1] addressed this challenge through the "rubber band model". This approach enabled time/frequency domain analysis of vehicle response at changing velocities. Their results demonstrated that acceleration PSD increases dramatically with vehicle speed, natural frequencies appear as velocity-independent peaks in response spectra, and RMS acceleration levels—which determine ride comfort—can be directly computed from integrated PSD.

Half-vehicle models extend vertical dynamics analysis by incorporating rotational degrees of freedom, enabling investigation of pitch (longitudinal plane) or roll (lateral plane) coupling with vertical motions. Karaçay and Aktürk [2] developed a 2-DOF half-vehicle trailer model incorporating heave and roll motion about the longitudinal axis. They fitted road PSD with analytical functions to characterize both low spatial frequencies (long wavelengths) and high spatial frequencies (short wavelengths). For resonant response near natural frequencies, narrow-band analysis s applied assuming an underdamped system. Their study specifically addressed cargo safety under stochastic road-induced vibrations, establishing quantitative relationships between trailer mass, vehicle speed, and the probability of exceeding critical acceleration thresholds (1g) that could cause cargo damage or weightlessness. Results indicated that light trailers (50 kg) exhibited ~55% probability of exceeding 1g at 80 km/h on standard roads, medium trailers (150 kg) showed ~7% probability, while heavy trailers (250 kg) demonstrated only ~1% probability at the same speed.

Eroğlu [3] extended the model complexity by adding 5-DOF lateral motion of car body and wheels to a 7-DOF longitudinal-vertical model, incorporating 2-DOF driver vertical and lateral motions, yielding a comprehensive 14-DOF full-vehicle formulation. However, this study employed simple sinusoidal road inputs rather than stochastic excitation, preventing investigation of realistic road roughness effects on coupled vehicle dynamics.

Wang [4] investigated battery mass distribution effects on electric vehicle safety using a 4-DOF half-car model focused on vertical dynamics. The study demonstrated that battery mounting location directly affects pitch natural frequency and mode shapes, with centrally-mounted battery packs providing optimal dynamic characteristics by minimizing pitch-heave coupling.

Recognizing limitations of linear models for large-displacement scenarios and accurate representation of suspension component characteristics, Özdemir and Erdoğan [5] developed a 7-DOF nonlinear half-vehicle suspension model focusing on optimal battery location for electric vehicles. Results demonstrated that front-mounted batteries increased pitch response and degraded ride quality, rear-mounted batteries exhibited similar pitch amplification, while centrally-mounted batteries minimized pitch-heave coupling with optimal performance achieved within ±200mm of geometric center. Additionally, cubic damping

improved high-velocity impact absorption, with nonlinear effects becoming critical for heavy EV battery packs exceeding 500 kg.

Eroğlu et al. [6] presented an 8-DOF full-vehicle model incorporating 1-DOF driver vertical displacement, specifically designed for comparative active suspension control analysis. The model enabled evaluation of control strategies characterized by simple implementation, three tunable parameters, and effectiveness for steady-state disturbance rejection, though with limited performance for complex multi-modal dynamics. This study also employed deterministic road inputs.

The stochastic nature of road surface roughness necessitates probabilistic analysis frameworks based on random process theory. Bendat and Piersol [7] established fundamental relationships for analyzing random data, including power spectral density (PSD), cross-spectral density for correlated left and right wheel track inputs, and input-output relations for linear systems with transfer functions. Newland [8] extended spectral analysis to multi-degree-of-freedom mechanical systems, developing transfer function matrices for MDOF systems, multi-input spectral analysis for systems with multiple correlated inputs, modal analysis of random vibration expressing response in terms of system modes, and time-varying system analysis for non-stationary random processes. These theoretical frameworks provide the foundation for converting spatial road profile measurements into temporal frequency-domain representations and computing vehicle response statistics.

The emergence of electric vehicles introduces concerns regarding vibration-induced degradation of sensitive components, particularly lithium-ion battery systems constituting significant vehicle mass and cost. Hua and Thomas [9] provided a comprehensive review examining dynamic loads and vibration effects on lithium-ion batteries across multiple applications, primarily identifying battery degradation concerns. Brand et al. [10] conducted standardized vibration tests (UN 38.3 T3 sine sweep, UN 38.3 T4 shock) on cylindrical 18650 cells, revealing that internal components such as electrodes can detach from proper mounting, causing intermittent electrical contact and progressive wear-accelerated degradation. Somerville et al. [11] demonstrated that solid-electrolyte interphase (SEI) layer disruption by vibration increases internal resistance and capacity fade. Consequently, vibration influence on discharge performance has been expressed by Hooper et al. [12,13] and Zhang et al. [14,15].

Vehicle dynamics under random road excitation has gained momentum in recent research, with studies addressing both structural vibration behavior and energy system performance. The vibration characteristics of structural components such as composite wings and UAV frames have been extensively analyzed through finite element methods to determine natural frequencies and mode shapes under various boundary conditions [16,17]. Simultaneously, the integration of electric vehicle battery systems into vehicle platforms requires consideration many parameter [18]. Lu [19] demonstrated that vibration amplitude is highly sensitive to small geometric variations, with optimal cell spacing significantly reducing pack-level resonance.

Hooper and Marco [20,21] measured actual vibration exposure in battery electric vehicles, identifying frequency-dependent contributions: low frequency (<10 Hz) dominated by vehicle body modes (heave, pitch, roll) providing dominant battery pack loading; medium frequency (10-50 Hz) associated with wheel hop and axle tramp modes; and high frequency (>200 Hz) attributable to power electronics switching noise, electric motor electromagnetic excitation, and cooling pump/fan rotation. Lang and Kjell [22] concluded that standard battery vibration tests remain inadequate for realistic EV conditions.

Despite extensive research on vehicle dynamics, such as adopt simplified quarter/half-car models or treat the battery pack as a symmetric and centric installed, a critical gap remains in the literature regarding studies that simultaneously integrate 7-DOF modeling, random road excitation, spectral analysis methods, and eccentric battery placement effects simultenously.

Hence, in this study, a novel comprehensive 7-DOF electrical vehicle dynamics model is presented with considering eccentric battery placement for analysing coupled pitch-roll-heave vibrations under random road excitation. To characterize how battery CG eccentricity influences vibration response, stochastic theory is used rather than deterministic approach, with including inter-DOF coupling across a wide speed range (~1–160 km/h). Thus, in realistic driving conditions, how battery CG eccentricity is affects PSD, FRF, displacement RMS, involving inter-DOF coupling, have been quantified. Real road profiles from the

UMTRI database are employed to characterize stochastic inputs. Spatial road roughness is transformed to vibration PSD's via FRF multiplication, providing a spectral prediction method. Therefore, the main contributions of this are establishing a combined 7-DOF formulation, the velocity-dependent resonance characteristics and cross-coupling amplification mechanisms that arise specifically from battery eccentricity and random road input in EVs. The proposed modeling approach, solution algorithm and results have direct practical significance for EV chassis design, battery/payload mounting optimization, and ride comfort assessment under realistic operating conditions.

2. MODELLING

2.1. Electrical Car Model with Battery Eccentricity

To obtain the vibration behavior of the electric vehicle, the vehicle dynamics modeling approach is adopted [23,24]. However, since battery eccentricity affects vehicle dynamics, this effect is taken into account in the developed model. Thus, a novel model is created within the scope of this study that it is enabling the investigation of the effects of battery eccentricity on vibration behavior and allowing the analysis of different payload positioning problems also. The geometric parameters and degrees of freedom for the developed model are shown in Figure 1(a,b).

Seven degrees of freedom are used in the modeling of the electric vehicle, with the vehicle body movement having 3 DoF (heave – z, roll – ϕ, pitch – θ) and each wheel vertical displacement movement (z_1, z_2, z_3, z_4) having one DoF. It is assumed that the battery is rigidly mounted within the x–y plane, with its eccentricity located at distances e and f from the CG along the x and y axes, respectively. In Figure 1(a), $u_1(t)$, $u_2(t)$, $u_3(t)$, $u_4(t)$ represent the road input.

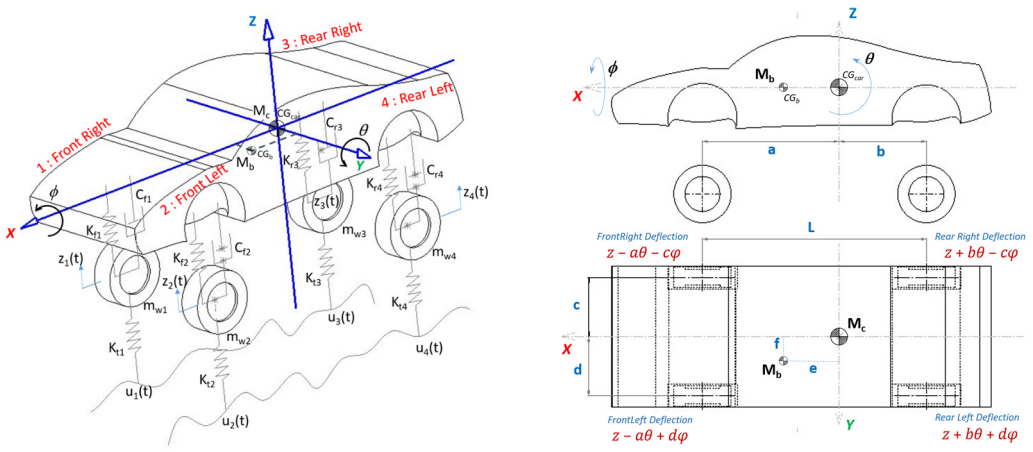

(a) (b)

Figure 1. Electrical Vehicle model (a) 7DoF with Eccentric Battery (b) geometry and corner displacements

The equations of motion are obtained from Newton's 2nd law as shown in Equations 1-7 by considering the electrical vehicle's deflections and rotation around static equilibrium position with small oscillations assumption.

$$\begin{aligned}&(M_c+M_b)\ddot{z}+(c_{f1}+c_{f2}+c_{r3}+c_{r4})\dot{z}+(k_{f1}+k_{f2}+k_{r3}+k_{r4})z\\&-[a(c_{f1}+c_{f2})-b(c_{r3}+c_{r4})]\dot{\theta}-[a(k_{f1}+k_{f2})-b(k_{r3}+k_{r4})]\theta\\&-[c(c_{f1}+c_{r3})-d(c_{f2}+c_{r4})]\dot{\phi}-[c(k_{f1}+k_{r3})-d(k_{f2}+k_{r4})]\phi\\&-c_{f1}\dot{z}_1-c_{f2}\dot{z}_2-c_{r3}\dot{z}_3-c_{r4}\dot{z}_4-k_{f1}z_1-k_{f2}z_2-k_{r3}z_3-k_{r4}z_4=0\end{aligned} \quad (1)$$

$$\begin{aligned}&(I_{xx}+M_bf^2)\ddot{\phi}-M_bef\ddot{\theta}\\&+[c^2(c_{f1}+c_{r3})+d^2(c_{f2}+c_{r4})]\dot{\phi}+[c^2(k_{f1}+k_{r3})+d^2(k_{f2}+k_{r4})]\phi\\&-[-c(ac_{f1}-bc_{r3})+d(ac_{f2}-bc_{r4})]\dot{\theta}-[-c(ak_{f1}-bk_{r3})+d(ak_{f2}-bk_{r4})]\theta\\&-[c(c_{f1}+c_{r3})-d(c_{f2}+c_{r4})]\dot{z}-[c(k_{f1}+k_{r3})-d(k_{f2}+k_{r4})]z\\&+cc_{f1}\dot{z}_1-dc_{f2}\dot{z}_2+cc_{r3}\dot{z}_3-dc_{r4}\dot{z}_4+ck_{f1}z_1-dk_{f2}z_2+ck_{r3}z_3-dk_{r4}z_4=0\end{aligned} \quad (2)$$

$$
\begin{aligned}
&(I_{yy}+M_b e^2)\ddot{\theta} - M_b ef\ddot{\phi} \\
&+\left[a^2(c_{f1}+c_{f2})+b^2(c_{r3}+c_{r4})\right]\dot{\theta} + \left[a^2(k_{f1}+k_{f2})+b^2(k_{r3}+k_{r4})\right]\theta \\
&-\left[-a(cc_{f1}-dc_{f2})+b(cc_{r3}-dc_{r4})\right]\dot{\phi} - \left[-a(ck_{f1}-dk_{f2})+b(ck_{r3}-dk_{r4})\right]\phi \\
&-\left[a(c_{f1}+c_{f2})-b(c_{r3}+c_{r4})\right]\dot{z} - \left[a(k_{f1}+k_{f2})-b(k_{r3}+k_{r4})\right]z \\
&+ac_{f1}\dot{z}_1 + ac_{f2}\dot{z}_2 - bc_{r3}\dot{z}_3 - bc_{r4}\dot{z}_4 + ak_{f1}z_1 + ak_{f2}z_2 - bk_{r3}z_3 - bk_{r4}z_4 = 0
\end{aligned} \tag{3}
$$

$$m_{w1}\ddot{z}_1 + c_{f1}\dot{z}_1 + (k_{f1}+k_{t1})z_1 - c_{f1}(\dot{z} - c\dot{\phi} - a\dot{\theta}) - k_{f1}(z - c\phi - a\theta) = k_{t1}u_1 \tag{4}$$

$$m_{w2}\ddot{z}_2 + c_{f2}\dot{z}_2 + (k_{f2}+k_{t2})z_2 - c_{f2}(\dot{z} + d\dot{\phi} - a\dot{\theta}) - k_{f2}(z + d\phi - a\theta) = k_{t2}u_2 \tag{5}$$

$$m_{w3}\ddot{z}_3 + c_{r3}\dot{z}_3 + (k_{r3}+k_{t3})z_3 - c_{r3}(\dot{z} - c\dot{\phi} + b\dot{\theta}) - k_{r3}(z - c\phi + b\theta) = k_{t3}u_3 \tag{6}$$

$$m_{w4}\ddot{z}_4 + c_{r4}\dot{z}_4 + (k_{r4}+k_{t4})z_4 - c_{r4}(\dot{z} + d\dot{\phi} + b\dot{\theta}) - k_{r4}(z + d\phi + b\theta) = k_{t4}u_4 \tag{7}$$

In modeling, mass, spring, and damping coefficients are denoted by the letters M or m, c, k, respectively. Subscripts are used to distinguish between parameters and variables. The relevant subscripts c, b, f, r, t are used to denote car, battery, front, rear, tire, respectively. The geometric parameters a, b, c, d, e, f, L are presented in Figure 1(b). If the equations of motion are written in matrix form as in Equation 8, the M, C, and K matrices will be as follows by using generalized coordinates as $\{q\}^T = \{z \quad \phi \quad \theta \quad z_1 \quad z_2 \quad z_3 \quad z_4\}$.

$$[M]\{\ddot{q}\} + [C]\{\dot{q}\} + [K]\{q\} = [F]\{u\} \tag{8}$$

where;

$$[M] = \begin{bmatrix} M_c+M_b & 0 & 0 & 0 & 0 & 0 & 0 \\ 0 & I_{xx}+M_b f^2 & -M_b ef & 0 & 0 & 0 & 0 \\ 0 & -M_b ef & I_{yy}+M_b e^2 & 0 & 0 & 0 & 0 \\ 0 & 0 & 0 & m_{w1} & 0 & 0 & 0 \\ 0 & 0 & 0 & 0 & m_{w2} & 0 & 0 \\ 0 & 0 & 0 & 0 & 0 & m_{w3} & 0 \\ 0 & 0 & 0 & 0 & 0 & 0 & m_{w4} \end{bmatrix}$$

$$[C] = \begin{bmatrix} C_{11} & C_{12} & C_{13} & -c_{f1} & -c_{f2} & -c_{r3} & -c_{r4} \\ C_{21} & C_{22} & C_{23} & cc_{f1} & -dc_{f2} & cc_{r3} & -dc_{r4} \\ C_{31} & C_{32} & C_{33} & ac_{f1} & ac_{f2} & -bc_{r3} & -bc_{r4} \\ -c_{f1} & cc_{f1} & ac_{f1} & c_{f1} & 0 & 0 & 0 \\ -c_{f2} & -dc_{f2} & ac_{f2} & 0 & c_{f2} & 0 & 0 \\ -c_{r3} & cc_{r3} & -bc_{r3} & 0 & 0 & c_{r3} & 0 \\ -c_{r4} & -dc_{r4} & -bc_{r4} & 0 & 0 & 0 & c_{r4} \end{bmatrix}$$

$$\begin{aligned}
C_{11} &= c_{f1}+c_{f2}+c_{r3}+c_{r4} \\
C_{12} = C_{21} &= -\left[c(c_{f1}+c_{r3}) - d(c_{f2}+c_{r4})\right] \\
C_{13} = C_{31} &= -\left[a(c_{f1}+c_{f2}) - b(c_{r3}+c_{r4})\right] \\
C_{22} &= c^2(c_{f1}+c_{r3}) + d^2(c_{f2}+c_{r4}) \\
C_{23} = C_{32} &= -\left[-c(ac_{f1}-bc_{r3}) + d(ac_{f2}-bc_{r4})\right] \\
C_{33} &= a^2(c_{f1}+c_{f2}) + b^2(c_{r3}+c_{r4})
\end{aligned}$$

$$[K] = \begin{bmatrix} K_{11} & K_{12} & K_{13} & -k_{f1} & -k_{f2} & -k_{r3} & -k_{r4} \\ K_{21} & K_{22} & K_{23} & ck_{f1} & -dk_{f2} & ck_{r3} & -dk_{r4} \\ K_{31} & K_{32} & K_{33} & ak_{f1} & ak_{f2} & -bk_{r3} & -bk_{r4} \\ -k_{f1} & ck_{f1} & ak_{f1} & k_{f1}+k_{t1} & 0 & 0 & 0 \\ -k_{f2} & -dk_{f2} & ak_{f2} & 0 & k_{f2}+k_{t2} & 0 & 0 \\ -k_{r3} & ck_{r3} & -bk_{r3} & 0 & 0 & k_{r3}+k_{t3} & 0 \\ -k_{r4} & -dk_{r4} & -bk_{r4} & 0 & 0 & 0 & k_{r4}+k_{t4} \end{bmatrix}$$

$$\begin{aligned}
K_{11} &= k_{f1}+k_{f2}+k_{r3}+k_{r4} \\
K_{12} = K_{21} &= -\left[c(k_{f1}+k_{r3}) - d(k_{f2}+k_{r4})\right] \\
K_{13} = K_{31} &= -\left[a(k_{f1}+k_{f2}) - b(k_{r3}+k_{r4})\right] \\
K_{22} &= c^2(k_{f1}+k_{r3}) + d^2(k_{f2}+k_{r4}) \\
K_{23} = K_{32} &= -\left[-c(ak_{f1}-bk_{r3}) + d(ak_{f2}-bk_{r4})\right] \\
K_{33} &= a^2(k_{f1}+k_{f2}) + b^2(k_{r3}+k_{r4})
\end{aligned}$$

$$[F] = \begin{bmatrix} 0 & 0 & 0 & 0 \\ 0 & 0 & 0 & 0 \\ 0 & 0 & 0 & 0 \\ k_{t1} & 0 & 0 & 0 \\ 0 & k_{t2} & 0 & 0 \\ 0 & 0 & k_{t3} & 0 \\ 0 & 0 & 0 & k_{t4} \end{bmatrix}$$

The static equilibrium position is calculated using the gravitational force matrix {W} and the [K] matrix, as in Equation 9, where $\{W\} = [-(M_c + M_b)g \quad -M_b gf \quad -M_b ge \quad -m_w g \quad -m_w g \quad -m_w g \quad -m_w g]^T$.

$$\{\delta_{st}\} = [K]^{-1}\{W\} \tag{9}$$

In MIMO systems, the system response can be obtained using approaches such as the transfer function, Laplace transform, convolution, or numerical solution methods, depending on the input. The relationship between the system input and the generalized coordinates, obtained by taking the Laplace transform of Equation 8, is shown in Equation 10. Here, [Q(s)] is the Laplace transform of the generalized coordinates, and [D(s)] is the dynamic stiffness matrix. Thus, the system response can be calculated using the transfer function G(s) with Equation 11 [25-27]. Since this study main objective heave, roll, and pitch motion relative to the road input, a [S] selection matrix is defined as [eye(3,3), zeros(3,4)].

$$\{Q(s)\} = \underbrace{(s^2[M] + s[C] + [K])^{-1}}_{D(s)}[F]\{U(s)\} \tag{10}$$

$$Y(s) = [S]\underbrace{[D(s)^{-1}][F]}_{G(s)}U(s) \tag{11}$$

Although Equation11 is commonly used for deterministic inputs, spectral methods are primarily used in random vibration analysis. In this study, the response of an electric vehicle with battery eccentricity to random road input is investigated using Equation 12 [7,8].

$$[S_{\gamma\gamma}(\omega)] = [H(\omega)][S_{uu}(\omega)][H(\omega)]^* \tag{12}$$

where, $[S_{\gamma\gamma}(\omega)]$, $[H(\omega)]$, $[S_{uu}(\omega)]$, $[H(\omega)]*$ are output PSD matrix, FRF matrix, input PSD matrix and complex conjugate transpose of FRF matrix respectively. Frequency Response Function (FRF) can be obtained substituting jω in Equation 13 [27].

$$[H(j\omega)] = \left[-\omega^2[M] + j\omega[C] + [K]\right]^{-1}[F] \tag{13}$$

Therefore, characteristic polynomial obtained as Equation 14.

$$\begin{aligned} &s^{14} + 169.9\,s^{13} + 2.924\times10^4\,s^{12} + 2.728\times10^6\,s^{11} + 2.408\times10^8\,s^{10} + 1.379\times10^{10}\,s^9 \\ &+7.357\times10^{11}\,s^8 + 2.472\times10^{13}\,s^7 + 7.692\times10^{14}\,s^6 + 1.142\times10^{16}\,s^5 + 1.665\times10^{17}\,s^4 \\ &+1.294\times10^{18}\,s^3 + 1.061\times10^{19}\,s^2 + 3.818\times10^{19}\,s + 1.765\times10^{20} = 0 \end{aligned} \tag{14}$$

2.2. Excitation Caused by Random Roughness Profile of Road

During real road driving, the right and left wheels will be subjected to separate road profile tracks. Therefore, UMTRI road data is used separately for the right and left wheels as the road model. However, between the front and rear wheels, there is also a phase delay depending on the vehicle's speed, and they are subjected to the same road profile. In other word, the right front wheel is exposed to the input representing the road roughness in Figure 2(a), and the same road input acting for the right rear wheel with a phase delay of σ time. Similarly, the left front wheel is exposed to the input representing the road roughness in Figure 2(a), and the same road input occurs at the left rear wheel with a phase delay of σ time.

Thus, the road profile spectral density S_{uu} is obtained using matrix in Equation15 and presented in Figure 2(b). Where, the auto-PSD S_{LL}, S_{RR}, and cross-PSD S_{LR}, S_{RL} of each road input can be calculated using Eqautions16-19 [8,25,26].

$$[S_{uu}(\omega)] = \begin{bmatrix} S_{LL}(\omega) & S_{LR}(\omega) & S_{LL}(\omega)e^{-j\omega\sigma} & S_{LR}(\omega)e^{-j\omega\sigma} \\ S_{LR}(\omega) & S_{RR}(\omega) & S_{LR}(\omega)e^{-j\omega\sigma} & S_{RR}(\omega)e^{-j\omega\sigma} \\ S_{LL}(\omega)e^{j\omega\sigma} & S_{LR}(\omega)e^{j\omega\sigma} & S_{LL}(\omega) & S_{LR}(\omega) \\ S_{LR}(\omega)e^{j\omega\sigma} & S_{RR}(\omega)e^{j\omega\sigma} & S_{LR}(\omega) & S_{RR}(\omega) \end{bmatrix} \tag{15}$$

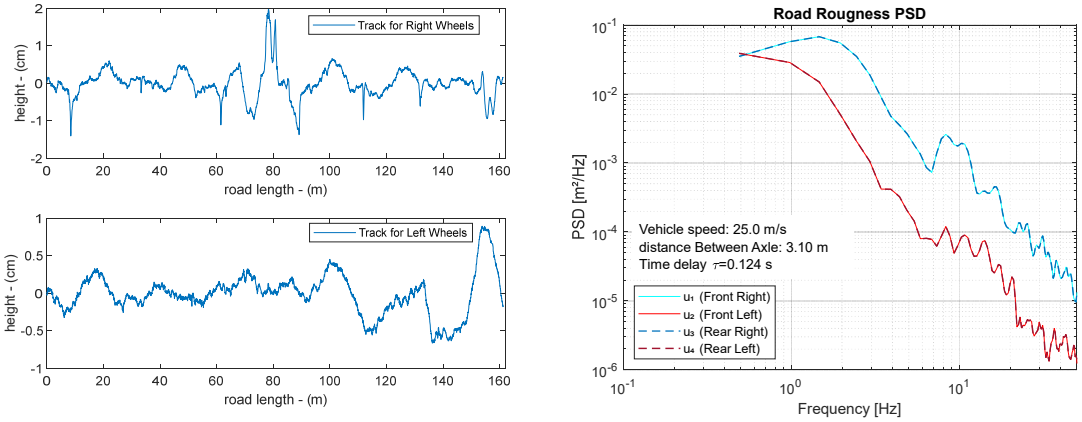

(a) (b)

Figure 2. Random Road Profile [28] (a) right wheels, (b) left wheels (c) PSD (S_{LL}, S_{RR})

$$S_{LL}(\omega) = \frac{1}{2\pi}\int_{-\infty}^{\infty}\left[\lim_{T\to\infty}\frac{1}{T}\int_0^T u_1(\sigma)u_1(\sigma+\tau)d\sigma\right]e^{-j\omega\tau}d\tau \quad (16)$$

$$S_{RR}(\omega) = \frac{1}{2\pi}\int_{-\infty}^{\infty}\left[\lim_{T\to\infty}\frac{1}{T}\int_0^T u_2(\sigma)u_2(\sigma+\tau)d\sigma\right]e^{-j\omega\tau}d\tau \quad (17)$$

$$S_{LR}(\omega) = \frac{1}{2\pi}\int_{-\infty}^{\infty}\left[\lim_{T\to\infty}\frac{1}{T}\int_0^T u_1(\sigma)u_2(\sigma+\tau)d\sigma\right]e^{-j\omega\tau}d\tau \quad (18)$$

$$S_{RL}(\omega) = \frac{1}{2\pi}\int_{-\infty}^{\infty}\left[\lim_{T\to\infty}\frac{1}{T}\int_0^T u_2(\sigma)u_1(\sigma+\tau)d\sigma\right]e^{-j\omega\tau}d\tau \quad (19)$$

where $\sigma = \frac{L}{V} = \frac{a+b}{V}$

3. NUMERICAL SIMULATION

The spectral method is used to obtain the response of the full vehicle model with battery eccentricity to the random road input. Hereby, the solution of Equation12 is obtained from the FRF and the road PSD. The vehicle displacement RMS values for the random road profile input is calculated from integration of the vehicle spectral response obtained from Equation12 wrt to the frequency vector. The system responses are obtained in the MATLAB by developed code for 9 separate battery eccentricity cases ans different vehicle speeds in increments of 1 m/s, in the speed range from 1 m/s to 45 m/s [~0 – 160 km/h]. Two separate road profiles are used for the right and left wheels.

The driving and battery eccentricity cases used in the simulation are presented in Table 1. Battery eccentricity is also shown in Figure 3. The parameters and values used for the numerical analysis are given in Table 2. The solution algorithm is given in Figure 4.

Table 1. Simulation cases

Case studies	Battery eccentricity	Eccentricity values		Speed (m/s)	Road profile
		e (m)	f (m)		
1	at car CG (concentric)	0.0	0.0	[1:1:46]	Profil-1 Profil-2
2	at Front Right	0.3	-0.2		
3	at Front Left	0.3	0.2		
4	at Rear Right	-0.3	-0.2		
5	at Rear Left	-0.3	0.2		
6	at Front Center (away from car CG)	0.6	0		
7	at Front Center (close to car CG)	0.3	0		
8	at Rear Center (close to car CG)	-0.3	0		
9	at Rear Center (away from car CG)	-0.6	0		

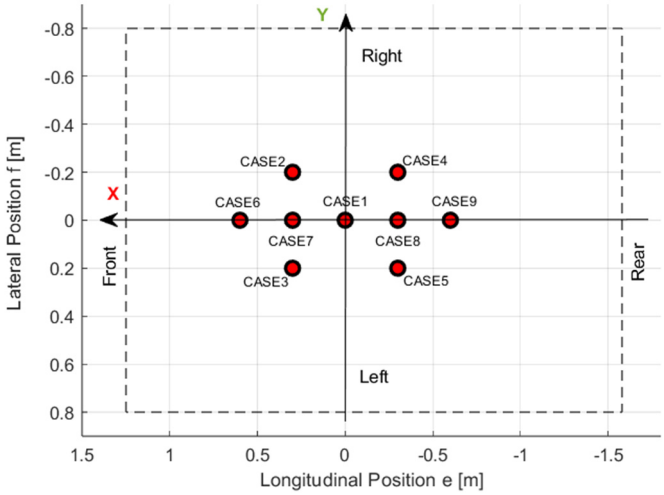

Figure 3. Battery eccentricity locations for each case

Table 2. Simulation data

Inertia			Geometry			Suspension damping			Suspension stiffness			Tire stiffness		
M_c	1500	kg	a	1.4	m	c_{f1}	1800	N·s/m	k_{f1}	25000	N/m	k_{t1}	180000	N/m
M_b	300	kg	b	1.7	m	c_{f2}	1800	N·s/m	k_{f2}	25000	N/m	k_{t2}	180000	N/m
I_{xx}	733.5	kg·m^2	c	0.8	m	c_{r3}	1600	N·s/m	k_{r3}	24000	N/m	k_{t3}	180000	N/m
I_{yy}	1806	kg·m^2	d	0.8	m	c_{r4}	1600	N·s/m	k_{r4}	24000	N/m	k_{t4}	180000	N/m
m_w	45	kg	h	1.5	m									

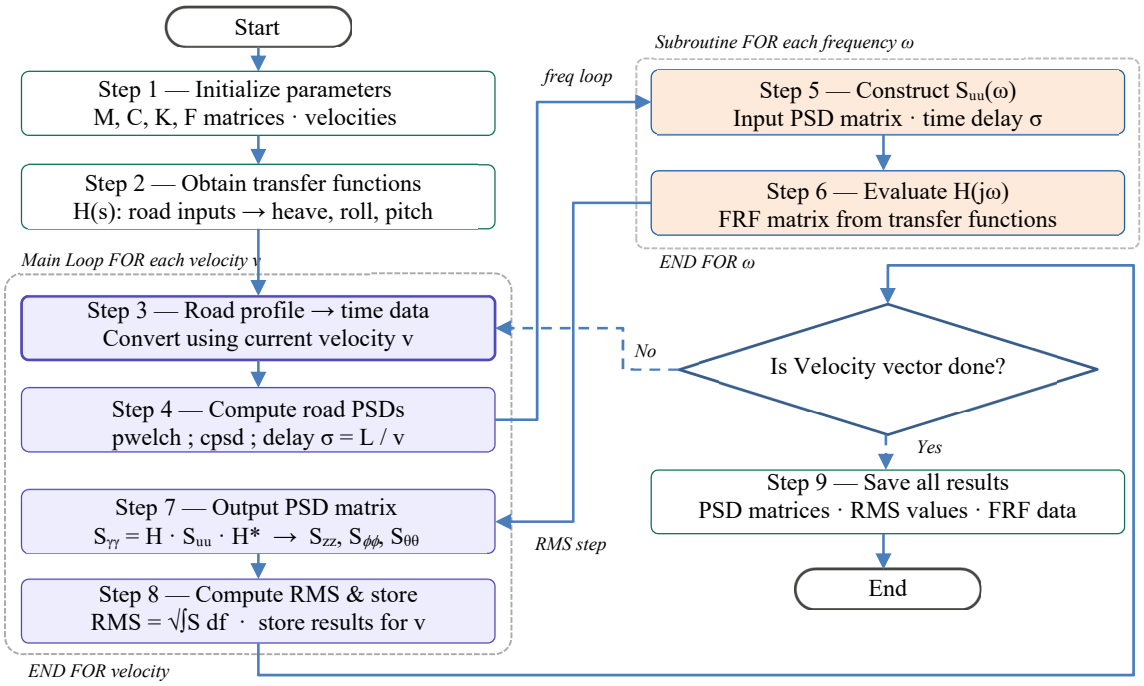

Figure 4. Flowchart of solution algorithm

4. RESULTS AND DISCUSSION

PSD graphs are presented in Figure 5. Here, there are speed-dependent frequencies and speed-independent fixed resonance frequencies. Speed-dependent frequencies are road-related, while speed-independent frequencies are vehicle-related frequencies, such as natural frequencies.

As seen in Figure 5, the vehicle displacement response PSD is high at low frequencies, and the displacement response PSD decreases with increased speed. A shoulder formed at the same frequency for all speed values in the PSD graphs contains harmonics that excite the vehicle's natural frequency. This peak located around 6 rad/s – 11 rad/s is indicates the natural frequency of the vehicle in heave-roll-pitch direction, while the peak occurring around 65 rad/s – 68 rad/s indicates the natural frequencies in the wheel z_1-z_4 direction. These peaks are more clearly visible in the Bode plot in Figure 6.

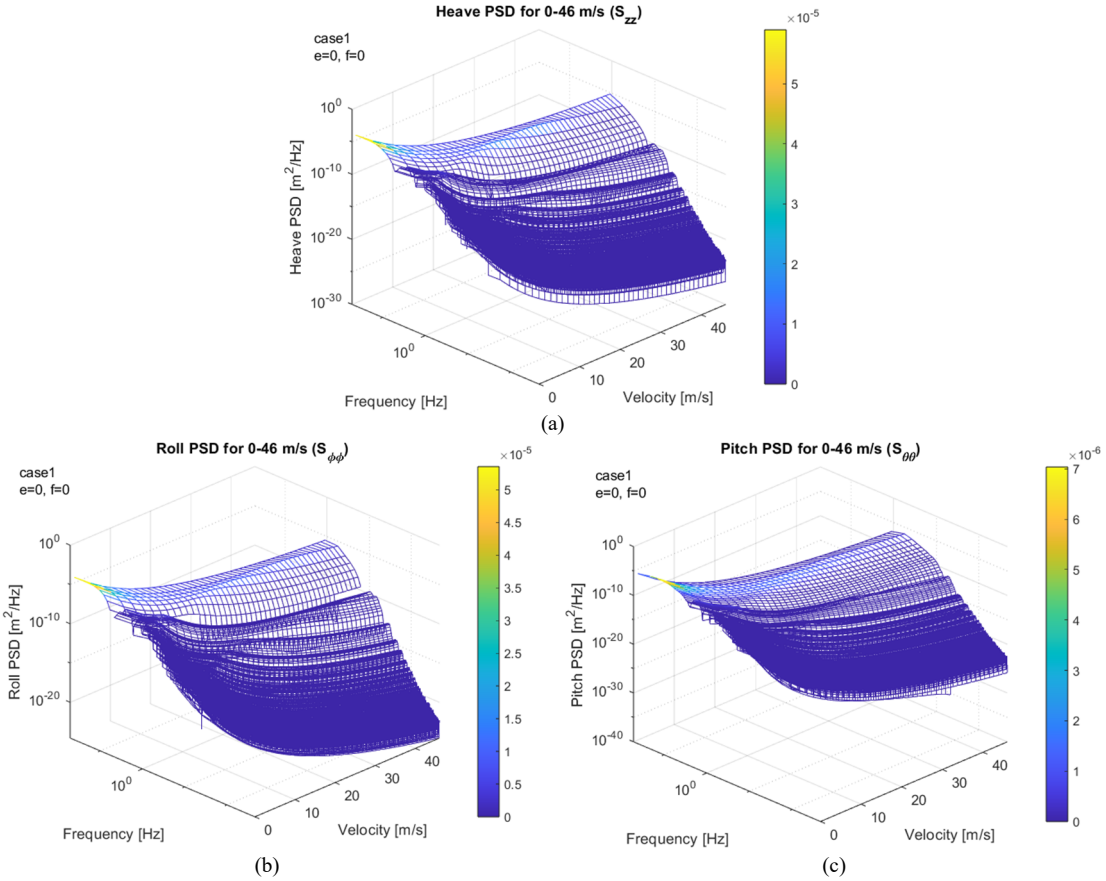

Figure 5. Response Power Spectral Density – PSD (*case1*) of (a) Heave motion, (b)Roll motion, (c) Pitch motion

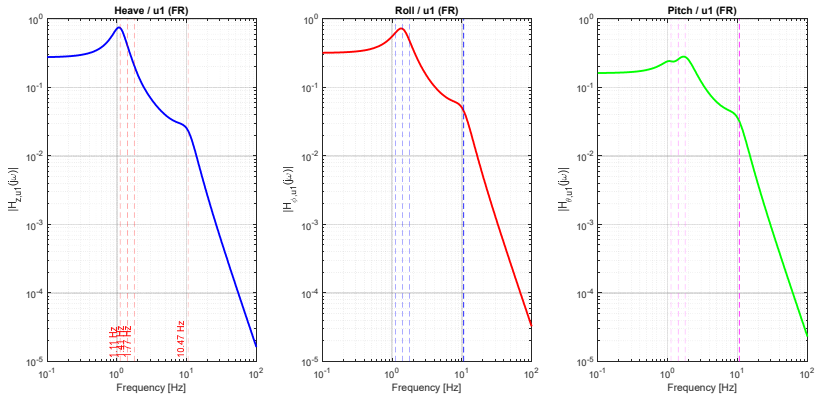

Figure 6. Frequency Response Function (FRF) magnitutes for road input u_1 (*case1*)

Since the displacement PSD of the road profile shows intensity in the low frequency range, the displacement response of the vehicle is seen to decrease with increasing frequency. The change in the displacement response PSD is given in Figure 7 for the specified speeds. Here, the decrease in PSD amplitude is seen to become more apparent as the natural frequency region is passed.

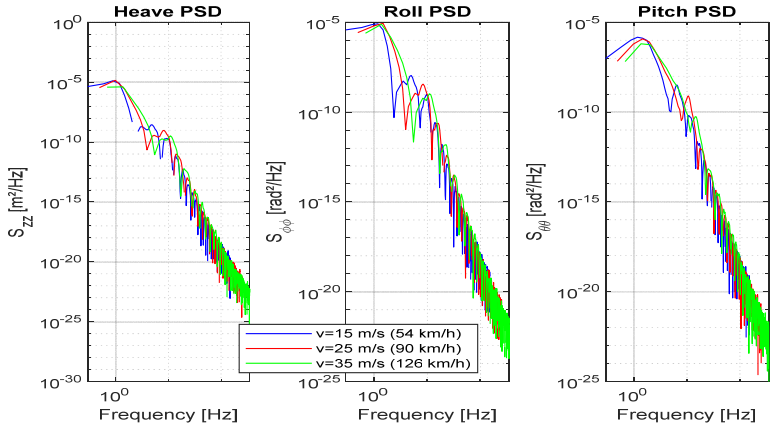

Figure 7. PSD magnitutes for different velocities (*case1*)

The RMS value of vehicle displacement can be calculated according to frequency using Equation 20 and it is represent the area under the PSD graphs. The use of RMS values instead of PSD is common in the literature. In this perspective, after obtaining response PSD's for all cases, the RMS values are calculated from the PSD's for each case study are presented in Figure 8.

$$x_{\mathrm{RMS}} = \sqrt{\int_{f_1}^{f_2} S_{xx}(f)\, df} \tag{20}$$

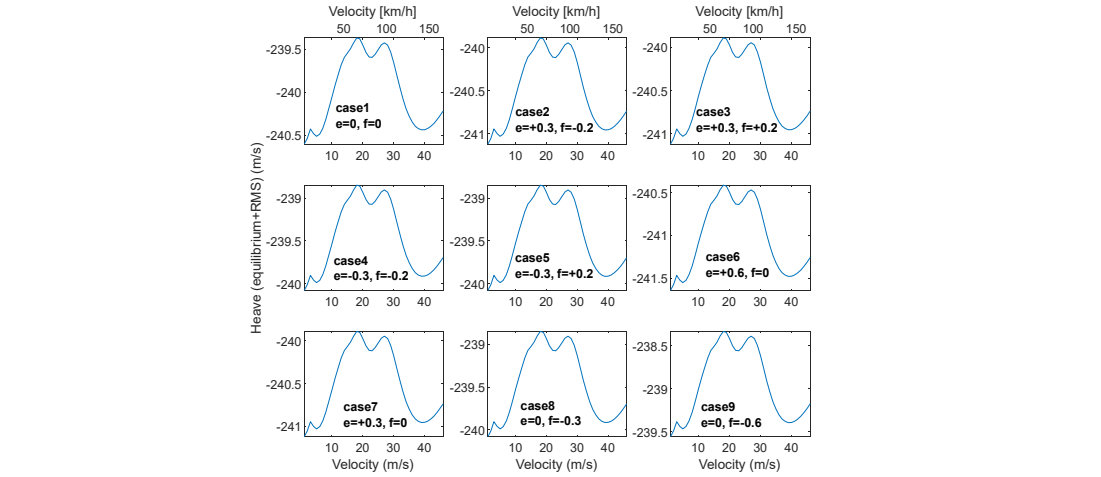

(a)

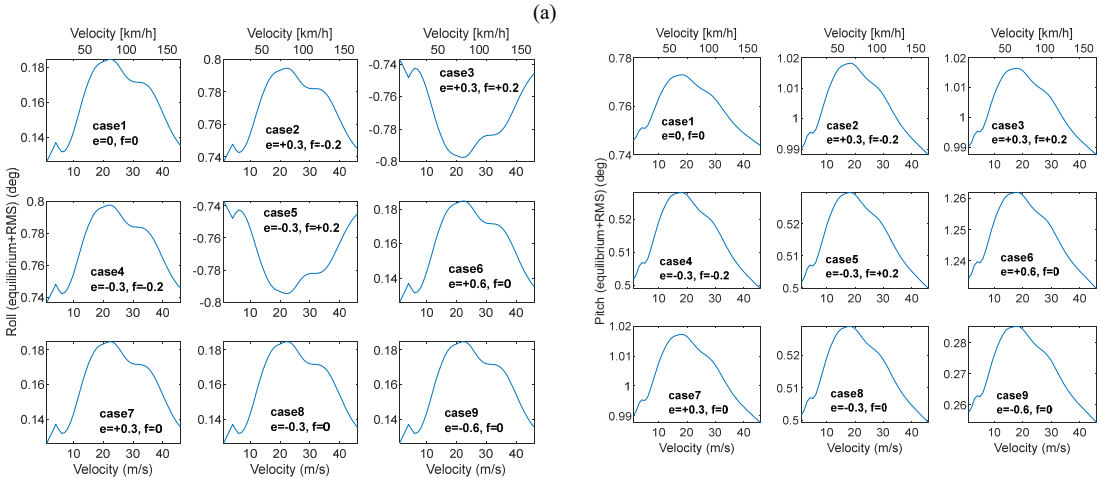

(b) (c)

Figure 8. Vibrations Root Mean Square – RMS values for all cases (a) Heave, (a) Roll, (c) Pitch

From the RMS graphs in Figure 8(a), it can be seen that maximum amplitudes occur at speeds of 18 m/s and 27 m/s for heave motion. Additionally, a local maximum is noticeable at 3 m/s. It is noted that amplitude increases occur at these speeds, particularly due to the excitation of natural frequencies between 1-3 Hz. This situation can also be seen in the PSD graph in Figure 5. However, it is observed in Figure 8(a) that the vehicle has different equilibrium points depending on the eccentricity of the battery and that the vehicle has heave roll and pitch oscillations around this equilibrium point. Results indicate that the smallest static equilibrium position is at -242.5 mm, where the battery eccentricity is at the -0.3 m in cases 4, 5, and 8. This is because the spring stiffness of the front and rear suspensions is different in the simulation and vehicle has positive pitch. The RMS amplitude of the dynamic oscillations is around 3.5 mm. These values will vary for different vehicle and battery masses and suspensions.

It is observed from Figure 8(b) that the Roll Motion RMS value differs particularly in case 3-5, which contains eccentricity (f=±0.2m) in the y direction. This is an expected result because the vehicle is symmetrical about the x-axis, and the eccentricity in the y direction changes the ± static equilibrium position. Local maximum amplitudes in the Roll motion RMS values are observed at speeds of 4 m/s, 22 m/s, and 34 m/s. It is evident in Figure 8(b) that the smallest Roll motion occurs when the battery CG is on the x-axis. The RMS amplitude of the dynamic oscillations is around 0.2 degrees.

Pitch RMS values for different battery eccentricities are presented in Figure 8(c). Local maximum values of 3 m/s and 18 m/s are observed in the pitch RMS value. This indicates that the pitch mode located 1 and 3 Hz interval, is excited by the road input at a vehicle speed of 18 m/s. Furthermore, it is observed that the variation of eccentricity on the x-axis mainly affects pitch oscillations, while the variation on the y-axis influences roll motion. Since, the vehicle CG is adjusted closer to the front of the vehicle configuration in the simulation, however, the stiffness and damping of the front and rear suspensions are selected differently. This creates a positive static equilibrium position for the pitch angle. Therefore, it is observed that the static equilibrium position decreased from 1.1844 degrees to 0.2076 degrees when the battery eccentricity shifts to the rear side. In addition, the RMS amplitude of the dynamic oscillations is determined to be around 0.1 degrees. These values are consistent with findings in the literature [1,29-31]. To compare the performance of the obtained results, the static equilibrium and dynamic RMS values are presented together in Figure 9(a,b).

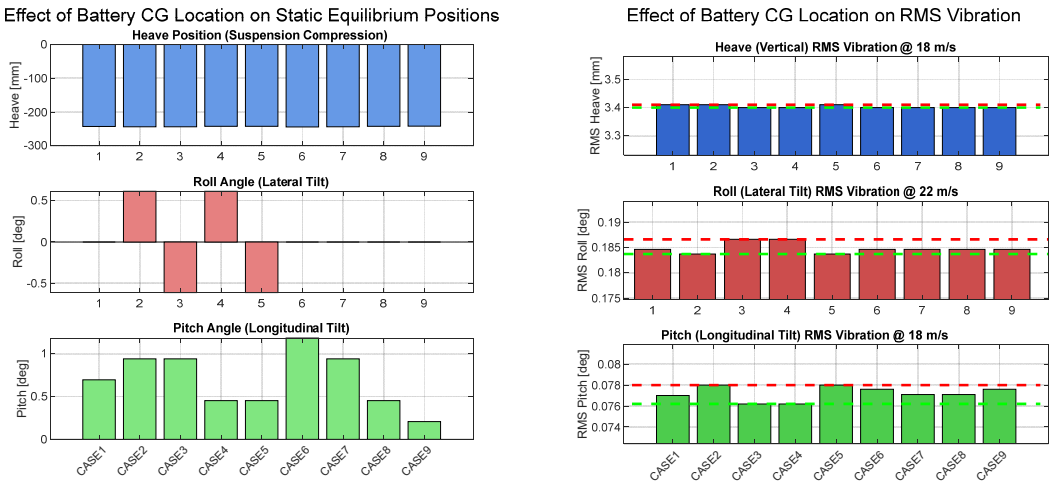

(a) (b)

Figure 9. Effect of the battery eccentricity on vibration (a) Static equilibrium position, (b) RMS amplitutes

The effect of battery eccentricity on vibration RMS amplitudes is more clearly illustrated in Figure 9. The variation of the battery CG location along the x- and y-axes shifts the vehicle's static equilibrium position toward the direction of eccentricity, as shown in Figure 9(a). Examining the RMS values in Figure 9(b), it is observed that the effect of road excitation on heave motion is approximately 3.5 mm. For roll motion RMS amplitutes are obtained approximately 0.185 degrees about the static equilibrium position. The pitch RMS demonstrate that Case 3 and Case 4 exhibit minimum oscillation, while higher amplitudes are obtained in Case 2 and Case 5. This behavior can be explained by the coupling between heave, roll, and pitch motions, besides the left and right wheels be subjected to different road excitations.

To clarify the results in terms of vibration performance, the RMS values are normalized using the expression ((x − min) / (max − min)). Based on these normalized RMS values, an integrated vibration index is calculated by summing the normalized motions. The lowest vibration index is observed in Case 1, Case 7, and Case 8. These cases indicate the conditions that battery eccentricity only along the x-axis and closest to the vehicle CG. The graph corresponding to the combined vibration index obtained through RMS normalization is presented in Figure 10. Results show that a 0.3 m eccentricity on the x-axis produces an increase of ~8% in the normalized RMS value, while eccentricity on both the 0.3 m x-axis and 0.2 m y-axis produces an increase of ~30% in the normalized total RMS value, from Figure 10.

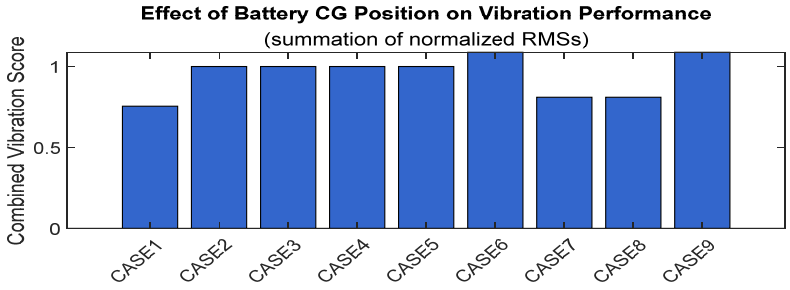

Figure 10. Compound vibration index

5. CONCLUSIONS

In this study, the effect of battery eccentricity variation on the vibration behavior of electric vehicles is investigated. For this purpose, an electirical vehicle with battery eccentricity is modelled with 7DoF. The heave, roll, and pitch vibrations of the derived electric vehicle model are calculated under random road excitation for different battery eccentricities and vehicle speeds using a spectral method. In the solution procedure, for each battery eccentricity, the vehicle displacement power spectral density is calculated for all vehicle speeds and corresponding frequencies by employing the road spectrum and FRF. Hereby, a method capable of determining the system response under nonstationary random inputs is presented, and the effect of battery CG position on vibration behavior is identified through the evaluation of vibration RMS values.

Results show that a 0.3 m eccentricity on the x-axis produces an increase of ~8% in the normalized RMS value, while eccentricity on both the 0.3 m x-axis and 0.2 m y-axis produces an increase of ~30% in the normalized RMS value. It is indicate that battery eccentricity or mounting imperfections has important contribution to vibtation response of EV. Therefore, it should be considered in vehicle dynamics response and riding comfort analysis.

The analyses related with vibration characteristics, yielded the following conclusions according to vehicle speed and different battery eccentricity:

- With vehicle speed increase, the displacement PSD decreases. High values occur within the natural frequency ranges of 6–11 rad/s and 65–68 rad/s. In the PSD diagram, it is observed as shoulder at these frequencies for all speeds.
- The highest PSD values are found at vehicle speeds of 3 m/s, 18 m/s, 22 m/s, and 27 m/s, corresponding to excitation near the vehicle's natural frequencies.
- The RMS values of random road excitation for heave, roll, and pitch motions are observed to be approximately 3.5 mm, 0.2 degrees, and 0.1 degrees, respectively. These values represent the RMS of vibrations about the static equilibrium position, which shifts significantly depending on battery eccentricity, as clearly shown in the graphs.
- The minimum roll motion occurs when the battery position lies along the x-axis.
- The RMS value of pitch oscillations increases as the battery position moves away from the vehicle CG. In addition, it is concluded that an increase in roll motion also influences pitch motion.
- Considering the vibration performance obtained from normalized RMS values, the optimal battery placement is achieved when the battery is located along the x-axis and close to the vehicle CG. Hence, Case 1, Case 7, and Case 8 correspond to the configurations with the lowest total vibration levels while Case 6 and Case 9 yields highest total vibration.

Finally, this paper contains following research potential as a future work; vibration reduction under the random road exitaion, bandwith improvement and resonance peak optimization, vibration control with different control action by employing active suspension, driving comfort for different payload position, vibration effect on state of charge and the life of the battery.

6. REFERENCES

1. Karaçay, T., Eroğlu, M. ve Aktürk, N. (2003). Gerçek yol girdisine maruz iki serbestlik dereceli çeyrek taşıt modelinin sürüş karakteristiğinin incelenmesi. *Gazi Üniversitesi Mühendislik Mimarlık Fakültesi Dergisi, 18*(4), 1-13.
2. Karaçay, T. & Aktürk, N. (2002). Bir römorkunun tasarımında gelişigüzel titreşimlerin etkisi. *Gazi Üniversitesi Mühendislik Mimarlık Fakültesi Dergisi, 17*(1), 11-30.
3. Eroğlu, M. (2022). Investigation of lateral and vertical direction dynamic responses of a full car model exposed to sine road input. *Sakarya University Journal of Science, 26*(4), 829-841.
4. Wang, P. (2020). Effect of electric battery mass distribution on electric vehicle movement safety. *Vibroengineering PROCEDIA, 33*, 78-83.
5. Özdemir, M. & Erdoğan, E.O. (2024). Determination of optimal battery locations for ride comfort in electric automobiles using a nonlinear half-vehicle suspension model. *Journal of the Faculty of Engineering and Architecture of Gazi University, 39*(1), 339-350.
6. Eroğlu, M., Koç, M.A., Kozan, R. & Esen, İ. (2022). Comparative analysis of full car model with driver using PID and LQR controllers. *International Journal of Automotive Science and Technology, 6*(2), 178-188.
7. Bendat, J.S., & Piersol, A.G. (2010). *Random data: Analysis and measurement procedures* (4th Ed). John Wiley & Sons, Hoboken, NJ, 2010.
8. Newland, D.E. (2012). *An introduction to random vibrations, spectral & wavelet analysis* (3rd Ed). Dover Publications, Mineola, NY, 2012.
9. Hua, X. & Thomas, A. (2021). Effect of dynamic loads and vibrations on lithium-ion batteries. *Journal of Low Frequency Noise, Vibration and Active Control, 40*(4), 1927-1934.
10. Brand, M.J., Schuster, S.F., Bach, T., Lorrmann, E., Jossen, A. & Quinger, D. (2015). Effects of vibrations and shocks on lithium-ion cells. *Journal of Power Sources, 288*, 62-69.
11. Somerville, L., Hooper, J.M., Marco, J., McGordon, A., Lyness, C., Walker, M. & Jennings, P. (2017). Impact of vibration on the surface film of lithium-ion cells. *Energies, 10*(6), 741.
12. Hooper, J.M., Marco, J., Chouchelamane, G.H., & Lyness, E.D. (2016). Vibration durability testing of nickel manganese cobalt oxide (NMC) lithium-ion 18650 battery cells. *Energies, 9*(1), 52.
13. Hooper, J.M., Marco, J., Chouchelamane, G.H., Lyness, E.D. & Taylor, J. (2018). Multi-axis vibration durability testing of lithium ion 18650 NCA cylindrical cells. *Journal of Energy Storage, 15*, 103-123.
14. Zhang, L., Ning, Z., Peng, H., Mu, Z. & Sun, C. (2017). Effects of vibration on the electrical performance of lithium-ion cells based on mathematical statistics. *Applied Sciences, 7*(8), 802.
15. Zhang, L., Mu, Z. & Gao, X. (2018). Coupling analysis and performance study of commercial 18650 lithium-ion batteries under conditions of temperature and vibration. *Energies, 11*(11), 2856.
16. Sarı, B., Kazemi Lichaei, M. & Yıldırım, S. (2022). Free vibration analysis of tapered composite aircraft wing via the finite element method. *Çukurova Üniversitesi Mühendislik Fakültesi Dergisi, 37*(3), 741-752.
17. Metin, M.A., Şentürk, K. ve Noorı, A.R. (2025). Hexacopter yapısındaki bir dron için gövde ana parçasının üç boyutlu sonlu elemanlar yöntemi ile serbest titreşim analizi. *Çukurova Üniversitesi Mühendislik Fakültesi Dergisi, 40*(2), 415-428.
18. Abdulvahitoğlu, A., Abdulvahitoğlu, A. ve Kılıç, M. (2022). Elektrikli araç bataryalarının bütünleşik Swara-Topsis metodu ile değerlendirilmesi. *Çukurova Üniversitesi Mühendislik Fakültesi Dergisi, 37*(4), 1061-1076.
19. Lu, J.C. (2018). Parametric reduced-order models for the structural dynamics of hybrid electric vehicle batteries. *PhD thesis.* University of Michigan, Ann Arbor, MI.
20. Hooper, J.M. & Marco, J. (2013). Understanding vibration frequencies experienced by electric vehicle batteries. *Proceedings of the IET Hybrid and Electric Vehicles Conference*, 1-6.

21. Hooper, J.M. & Marco, J. (2014). Characterising the in-vehicle vibration inputs to the high voltage battery of an electric vehicle. *Journal of Power Sources, 245*, 510-519.
22. Lang, J.F. & Kjell, G. (2015). Comparing vibration measurements in an electric vehicle with standard vibration requirements for Li-ion batteries using power spectral density analysis. *International Journal of Electric and Hybrid Vehicles, 7*(3), 272-286.
23. Wong, J.Y. (2022). *Theory of ground vehicles.* John Wiley & Sons.
24. Jazar, R.N. (2025). *Vehicle dynamics: theory and application.* Springer Nature.
25. Rao, S.S. & Yap, F.F. (1995). *Mechanical vibrations.* Addison-Wesley New York.
26. Inman, D.J. & Singh, R.C. (1994). *Engineering vibration.* Prentice Hall Englewood Cliffs, NJ.
27. Ogata, K. (2020). *Modern control engineering.* Prentice Hall, NJ.
28. University of Michigan Transportation Research Institute (UMTRI) (2023). *Road profile measurement database.* Available: www.umtri.umich.edu, Ann Arbor, MI.
29. Bakar, S.A.A., Masuda, R., Hashimoto, H., Inaba, T., Jamaluddin, H., Rahman, R.A. & Samin, P.M. (2012). Ride comfort performance of electric vehicle conversion with active suspension system. *Proceedings of SICE Annual Conference (SICE),* 1980-1985.
30. Dumitriu, D., Chiroiu, V. & Munteanu, L. (2015). Simplified 7 DOF model of car vertical vibrations for small pitch and roll angles. *Applied Mechanics and Materials, 801*, 136-141.
31. Sulaiman, S., Samin, P.M., Jamaluddin, H., Rahman, R.A. & Burhaumudin, M.S. (2012). Modeling and validation of 7-DOF ride model for heavy vehicle. *Proceedings of the ICAMME*.